

Multimodal Lead-Specific Modeling of ECG for Low-Cost Pulmonary Hypertension Assessment

Mohammad N. I. Suvon^{1,2}(✉), Shuo Zhou^{1,2}, Prasun C. Tripathi^{1,7}, Wenrui Fan^{1,2}, Samer Alabed^{3,4,5}, Bishesh Khanal⁹, Venet Osmani⁶, Andrew J. Swift^{3,4,5}, Chen (Cherise) Chen^{1,8,10}, and Haiping Lu^{1,2,5}

¹ Department of Computer Science, University of Sheffield, Sheffield, UK

² Centre for Machine Intelligence, University of Sheffield, Sheffield, UK

³ Department of Infection, Immunity and Cardiovascular Disease, University of Sheffield, Sheffield, UK

⁴ Department of Clinical Radiology, Sheffield Teaching Hospitals, Sheffield, UK

⁵ INSIGNEO, Institute for in Silico Medicine, University of Sheffield, Sheffield, UK

⁶ Digital Environment Research Institute, Queen Mary University of London, London, UK

⁷ Department of Computer Science, IITRAM, Gujarat, India

⁸ Nepal Applied Mathematics and Informatics Institute for research (NAAMII), Nepal

⁹ Department of Engineering Science, University of Oxford, Oxford, UK

¹⁰ Department of Computing, Imperial College London, London, UK

{m.suvon^(✉), shuo.zhou, p.c.tripathi, wenrui.fan, s.alabed, a.j.swift, chen.chen2, h.lu}@sheffield.ac.uk, v.osmani@qmul.ac.uk, bishesh.khanal@naamii.org.np

Abstract. Pulmonary hypertension (PH) is frequently underdiagnosed in low- and middle-income countries (LMICs) primarily due to the scarcity of advanced diagnostic tools. Several studies in PH have applied machine learning to low-cost diagnostic tools like 12-lead ECG (12L-ECG), but they mainly focus on areas with limited resources, overlooking areas with no diagnostic tools, such as rural primary healthcare in LMICs. Recent studies have shown the effectiveness of 6-lead ECG (6L-ECG), as a cheaper and portable alternative in detecting various cardiac conditions, but its clinical value for PH detection is not well proved. Furthermore, existing methods treat 12L-/6L-ECG as a single modality, capturing only shared features while overlooking lead-specific features essential for identifying complex cardiac hemodynamic changes. In this paper, we propose **Lead-Specific Electrocardiogram Multimodal Variational Autoencoder (LS-EMVAE)**, a model pre-trained on large-population 12L-ECG data and fine-tuned on task-specific data (12L-ECG or 6L-ECG). LS-EMVAE treats each lead in 12L-ECG as a separate modality and incorporates a novel hierarchical modality expert composition mechanism based on Mixture of Expert and Product of Expert to enable flexible, adaptive latent feature fusion among lead-specific and shared features. Unlike existing approaches, LS-EMVAE makes better predictions on both 12L-ECG and 6L-ECG at inference time, making it an equitable solution for areas with both limited and no diagnostic tools. We pre-trained LS-EMVAE on 800,000 publicly available 12L-ECG samples and fine-tuned

it for two tasks: 1) PH detection and 2) phenotyping pre-/post-capillary PH, on in-house datasets of 892 and 691 subjects across 12L-ECG and 6L-ECG settings. Extensive experiments show that LS-EMVAE outperforms existing baselines in both ECG settings, while 6L-ECG achieves performance comparable to 12L-ECG, unlocking its potential for global PH screening in areas without diagnostic tools.

Keywords: Pulmonary hypertension, Variational autoencoder, Multi-modal learning

1 Introduction

Pulmonary Hypertension (PH) is a complex and heterogeneous condition that affects approximately 75 million individuals worldwide [14]. PH can be precisely measured using right heart catheterization (RHC), an invasive and expensive procedure to assess cardiac hemodynamics, including two surrogate markers: mean pulmonary arterial pressure (mPAP) and pulmonary artery wedge pressure (PAWP) for PH detection and phenotyping pre-/post-capillary PH.

In recent years, many machine-learning based methods were developed to predict cardiac hemodynamics non-invasively using high-cost, high-precision imaging techniques like cardiac magnetic resonance imaging (MRI) [24,25] and echocardiography [23], as well as more affordable and accessible diagnostic tools such as 12-lead electrocardiogram (12L-ECG) [17] and chest X-rays (CXR) [10]. For instance, Suvon et al. [22] demonstrated that CXR and 12L-ECG can be used to detect cardiac hemodynamics instability (CHDI). Using multimodal learning, this method achieved comparable performance to cardiac MRI in detecting CHDI. Notably, in unimodal studies, 12L-ECG outperformed CXR, underscoring its effectiveness in predicting cardiac hemodynamics.

Most of the aforementioned studies assume advanced diagnostics such as cardiac MRI or at least low-cost diagnostics like 12L-ECG are available. However, in LMICs, nearly 80% cases of PH remain undiagnosed due to the lack of diagnostic tools [14]. In these areas, clinicians often rely on symptom-based evaluation, emphasizing the need for easily implementable and low-cost portable diagnostic tools like 6-lead ECG device [2], which captures six limb leads (I, II, III, aVR, aVL, aVF). More recently, some pre-training methods have shown effectiveness in predicting various cardiac conditions using 6L-ECG [15,29]. For instance, Na et al. [15] introduced an ST-MEM model using a vision transformer (ViT) and a masked autoencoder (MAE) to capture spatiotemporal features in 12-lead ECG signals. They further demonstrated its adaptability to 6-lead ECGs for predicting atrial fibrillation (AF).

Despite these advancements, existing methods face two main challenges. *Firstly*, they fuse features through raw data fusion [26] or attention-based fusion [29], restricting spatial relationships between leads and focusing only on shared features in the latent space, which impacts prediction performance. While shared features from 12L-ECG may be enough for simpler tasks like AF prediction, PH involves more complex cardiac hemodynamic changes [6] that require

both lead-specific and shared features with proper alignment. *Secondly*, most baselines treat 12L-ECG as a single modality, where each lead contributes equally to the model. However, in complex diseases like PH, certain leads are more important. For example, in PH detection with 6L-ECG, *Lead-II is more important* as it offers the clearest view of atrial depolarization (the P wave), enabling the detection of right atrial enlargement and pressure changes [6].

To address the above challenges, we propose lead-specific electrocardiogram multimodal variational autoencoder (LS-EMVAE) pre-training model based on the MVAE [28] architecture. The **main contributions** of this paper are three-fold: 1) Unlike previous methods that treat the entire 12L-ECG as a single modality and focus only on shared features, we propose LS-EMVAE, a pre-training model that considers each lead as a separate modality and simultaneously learns lead-specific and shared features. 2) We introduce a novel latent distribution parameter fusion strategy. In addition to the standard Mixture of Experts (MoE) [18] for multimodal feature fusion, we introduce Product of Experts (PoE) [8] to better integrate features from different leads. This strategy also includes a cross-modality alignment regularization loss to improve alignment between lead-specific and shared features in latent space. Unlike previous methods that treat all leads contribution equally, our fusion strategy uses adaptive weights to control each lead’s contribution, which is crucial for PH detection. This strategy further enables LS-EMVAE to adapt to 6L-ECG settings, providing a cost-effective solution for areas without diagnostic tools, enabling faster and easier PH screening. 3) Through extensive experiments, we show that LS-EMVAE outperforms both unimodal and multimodal baselines in 12L-ECG and 6L-ECG settings. We further perform ablation studies and model interpretation to assess key components of our model and visualize explainable clinical features, enhancing its practical use and effectiveness in real-world scenarios.

2 Methods

Fig. 1(c) illustrates the architecture of our proposed LS-EMVAE, which consists of 12 encoders, a latent distribution parameter fusion method, and a shared decoder. Below, we describe each building block of our model.

Encoder Design: In our encoder, each lead in the 12-lead ECG is treated as a separate modality and encoded independently using a convolutional neural network (CNN), resulting in 12 separate encoders, one for each lead. Each encoder consists of three 1D convolutional layers, each configured with a kernel size of 3, stride of 2, and padding of 1, followed by ReLU activations. Following this, the data is flattened and passed through two fully connected layers, with each encoder outputting the latent distribution parameter experts (μ_i, σ_i) , where i corresponds to each lead in $\{I, II, III, aVR, aVL, aVF, V_1-V_6\}$.

Latent Distribution Parameter Fusion: In latent distribution parameter fusion (Fig. 1(d)), we use PoE [8] and MoE [18] to integrate latent distribution parameters for learning both lead-specific and shared features. First, each lead-specific latent distribution parameters μ_i and σ_i is combined using PoE [8] to

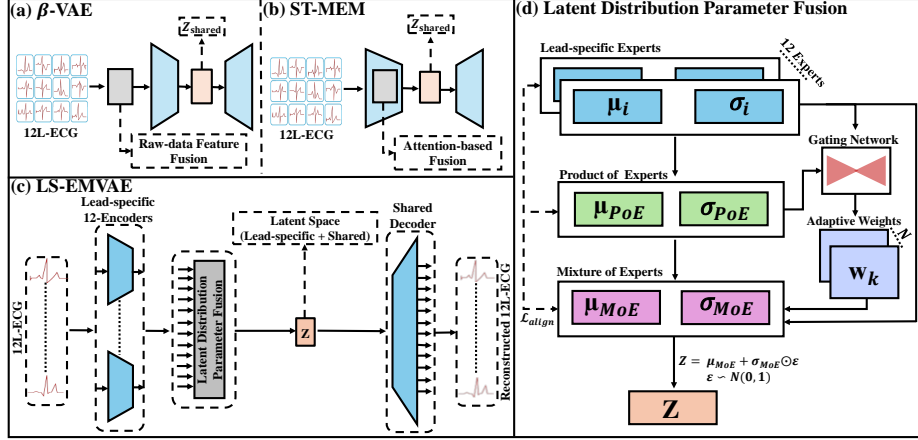


Fig. 1: The pre-training baselines and proposed LS-EMVAE pre-training architecture. (a, b) Top left: the raw-data feature fusion baseline β -VAE [26] and the attention-based feature fusion baseline ST-MEM [15], which utilize only the shared features in the latent space. (c) Bottom left: An overview of our proposed LS-EMVAE pre-training model. (d) Right: latent distribution parameter fusion method to learn both lead-specific and shared features and create a better alignment between them in the latent space. Here, i denotes the ECG lead (I, II, III, aVR, aVL, aVF, V_1 – V_6), k denotes each expert, and N represents the number of experts.

compute shared expert (μ_{PoE}, σ_{PoE}): $\mu_{PoE} = (\sum_{i=1}^N \mu_i / \sigma_i^2) / (\sum_{i=1}^N 1 / \sigma_i^2)$ and $\sigma_{PoE}^2 = 1 / (\sum_{i=1}^N 1 / \sigma_i^2)$. Second, both lead-specific and shared experts pass through a gating mechanism [18] to compute adaptive weights w_k , where k represents latent distribution parameter experts *including both lead-specific and shared experts*. Finally, using MoE[18], these learned adaptive weights, along with all k experts, are used to compute (μ_{MoE}, σ_{MoE}): $\mu_{MoE} = \sum_{k=1}^N w_k \cdot \mu_k$, $\sigma_{MoE}^2 = \sum_{k=1}^N w_k \cdot (\sigma_k^2 + \mu_k^2) - \mu_{MoE}^2$. Next, we introduce a cross-modality alignment regularization loss $\mathcal{L}_{\text{align}}$ to ensure that each expert’s latent distribution parameter μ_k is better aligned with μ_{MoE} . The loss is defined as:

$$\mathcal{L}_{\text{align}} = \gamma \cdot \frac{1}{N} \sum_{k=1}^N \|\mu_k - \mu_{MoE}\|_2^2 \quad (1)$$

where N is the number of experts and γ is a hyperparameter that controls the strength of regularization, enabling tuning of cross-modality alignment during pre-training. Finally, the latent space Z is sampled using the reparameterization trick $Z = \mu_{MoE} + \sigma_{MoE} \cdot \epsilon$, where ϵ follows a standard Gaussian distribution $\mathcal{N}(0, \mathbf{I})$, acting as a prior for the latent space.

Decoder Design: In our decoder, we employ a shared decoder to reconstruct each lead of the 12-lead ECG from the latent space Z . For each lead, the shared

decoder reconstructs the corresponding lead signal. The decoder consists of a fully connected layer that expands the latent representation, followed by three 1D transposed convolutional layers with kernel size 4, stride 2, and padding 1. These layers progressively restore the temporal structure of the corresponding ECG lead signal. The final layer applies an identity activation [4], ensuring the reconstructed waveform maintains the correct amplitude scale.

Pre-training Paradigm: In pre-training, we process each lead of the 12L-ECG separately through our LS-EMVAE model and compute the Evidence Lower Bound (ELBO) [21] loss, which is defined as:

$$\mathcal{L}_{\text{ELBO}} = \underbrace{\sum_{i=1}^N \lambda_i \cdot \mathcal{L}_{\text{MSE}_i}}_{\text{Reconstruction Loss}} + \underbrace{\beta \cdot \frac{1}{2} (\mu_{\text{MoE}}^2 + \sigma_{\text{MoE}}^2 - \ln(\sigma_{\text{MoE}}^2) - 1)}_{\text{KL Divergence Loss}}. \quad (2)$$

where N represents the number of leads, and the first part of the loss corresponds to the reconstruction loss, while the second part is the Kullback-Leibler (KL) divergence loss [3]. Two hyperparameters, λ_{ECG_i} [11] and β [7], are introduced to balance the reconstruction loss across leads and regulate the trade-off between reconstruction and KL divergence, respectively. During pre-training, $\lambda_{\text{ECG}_i} = 1$ for all leads, and β is gradually increased from 0 to 1 to establish a valid lower bound on the evidence [1]. The total loss is then obtained by combining Eq. (1) and Eq. (2), formulated as $\mathcal{L}_{\text{total}} = \mathcal{L}_{\text{ELBO}} + \mathcal{L}_{\text{align}}$. We optimize this total loss to jointly learn lead-specific and shared representations while ensuring cross-modality alignment in the latent space Z .

Fine-tuning Strategy: Fine-tuning the pre-trained model is straightforward, as it retains both lead-specific and shared information through a latent distribution parameter fusion strategy. During fine-tuning, the new downstream dataset is passed through the frozen model, which is then processed by two fully connected layers for the final prediction. To address class imbalance in downstream tasks, we fine-tune the model using focal loss [12]. The pre-trained LS-EMVAE model has 256M trainable parameters.

3 Experimental Results and Analysis

Dataset for Pre-training: We pre-trained LS-EMVAE model using the MIMIC-IV-ECG dataset [5], including 800,000 ECGs from 160,000 unique patients.

Study Population and Dataset for Downstream Task: We evaluated all models using our in-house dataset for two downstream tasks: PH detection and phenotyping pre-/post-capillary PH. The study was approved by the local institutional review board and ethics committee. It included a total of 892 patients who underwent RHC and 12L-ECG. Based on the measurements from RHC (using a balloon-tipped 7.5 French thermodilution catheter), we identified 201 healthy patients and 691 patients with PH for the PH detection task. For the pre-/post-capillary PH phenotyping task, among the 691 PH patients, 555 had

Table 1: Patient characteristics of included patients in our in-house dataset. p -values were obtained using Welch’s t -test [27].

| | Non-PH (mPAP \leq 20) | PH (mPAP $>$ 20) | p -value (mPAP) | Pre-capillary PH (PAWP \leq 15) | Post-capillary PH (PAWP $>$ 15) | p -value (PAWP) |
|--|----------------------------|---------------------|----------------------|--------------------------------------|------------------------------------|----------------------|
| Number of patients | 201 | 691 | – | 136 | 555 | – |
| Age (years) | 58.43 \pm 11.64 | 65.41 \pm 13.02 | $<$ 0.0001 | 61.56 \pm 14.7 | 69.26 \pm 11.34 | $<$ 0.0001 |
| Body Surface Area | 1.89 \pm 0.21 | 1.93 \pm 0.26 | 0.03 | 1.89 \pm 0.24 | 1.97 \pm 0.28 | 0.001 |
| Heart Rate (bpm) | 68.86 \pm 8.42 | 76.94 \pm 13.99 | $<$ 0.0001 | 79.34 \pm 14.14 | 74.55 \pm 13.84 | 0.0005 |
| Pulmonary Artery Systolic Pressure | 72.75 \pm 19.56 | 74.42 \pm 21.64 | 0.04 | 72.53 \pm 20.53 | 76.31 \pm 22.75 | 0.06 |
| Pulmonary Artery Diastolic Pressure | 22.54 \pm 9.43 | 24.54 \pm 10.23 | 0.009 | 23.27 \pm 11.53 | 25.45 \pm 8.93 | 0.04 |
| mPAP | 14.23 \pm 4.31 | 26.82 \pm 5.14 | $<$ 0.0001 | 25.32 \pm 3.86 | 28.33 \pm 6.43 | $<$ 0.0001 |
| PAWP | 13.67 \pm 6.77 | 16.38 \pm 3.81 | $<$ 0.0001 | 11.23 \pm 2.98 | 21.53 \pm 4.65 | $<$ 0.0001 |

pre-capillary PH and 136 had post-capillary PH. Table 1 provides an overview of the patient characteristics from our in-house dataset.

Experimental Design: We pre-trained our LS-EMVAE model using the MIMIC-IV-ECG dataset [5], partitioning it with a 90 : 10 ratio for training and validation. The hyperparameters λ_{ECG_i} , β , and γ were selected using grid search. The optimal hyperparameters were then used to pre-train the LS-EMVAE model on the entire MIMIC-IV-ECG dataset. The latent dimension was set to 256. For optimization, we used the AdamW [13] optimizer with a learning rate of 1×10^{-4} and a batch size of 128, training for 100 epochs to ensure model convergence.

For fine-tuning, we used two experimental settings: 6L-ECG and 12L-ECG. The encoder layers were frozen, and only the fully connected (FC) layers were fine-tuned for both ECG settings. We used 128 nodes in the FC layer and applied a dropout of 0.5. We evaluated the prediction performance using 5-fold cross-validation with a training and validation ratio of 80 : 20. We set the learning rate to 1×10^{-4} and the batch size to 32, training the model for 50 epochs. We assessed classification performance using Area Under Receiver Operating Curve (AUROC), Matthews correlation coefficient (MCC), and accuracy. For a fair comparison, we used the same training settings and data partitioning for comparing methods [9,19,26,15,28,21]. An Nvidia A100 GPU with 256GB RAM was used for all experiments. The implementation of all models was carried out in Python (version 3.11) with PyTorch (version 2.1.2) [16].

Unimodal Method Study: Table 2 compares LS-EMVAE against four competitive unimodal method baselines, including two without pre-training and two with pre-training. From Table 2, it is clear that, ST-MEM is the strongest unimodal method baseline, but XResNet1D without pre-training, a top-performing network architecture for ECG analysis [19], achieves comparable performance. β -VAE model applies raw-data feature fusion by combining all 12 leads before encoding, while ST-MEM uses ViT and performs attention-based fusion. Our LS-EMVAE outperforms these two methods. The results on 12L-ECG setting show that LS-EMVAE obtains improvements of Δ Accuracy = 0.013, Δ AUROC = 0.028, and Δ MCC = 0.059 on PH detection and Δ Accuracy = 0.003, Δ AUROC = 0.047, and Δ MCC = 0.169 on PH phenotyping. A similar pattern is observed

Table 2: Performance comparison across two downstream tasks: Task 1 (PH detection) and Task 2 (phenotyping pre-capillary and post-capillary PH), based on Accuracy, AUROC, and MCC metrics, in two ECG settings: 6L- and 12L-ECG. The overall **best** results are highlighted in **bold** and the best result in unimodal study are marked in underline.

| Study Type | Method | Pre-training | Accuracy | | AUROC | | MCC | |
|---|-------------------|--------------|------------------------------------|------------------------------------|------------------------------------|------------------------------------|------------------------------------|------------------------------------|
| | | | 12L | 6L | 12L | 6L | 12L | 6L |
| Task-1: PH detection | | | | | | | | |
| Unimodal | Resnet1d [9] | \times | 0.744 ± 0.06 | 0.750 ± 0.05 | 0.798 ± 0.03 | 0.763 ± 0.05 | 0.315 ± 0.10 | 0.242 ± 0.09 |
| | xResnet1d [19] | \times | 0.804 ± 0.01 | 0.772 ± 0.01 | 0.816 ± 0.02 | 0.796 ± 0.03 | 0.387 ± 0.09 | 0.188 ± 0.08 |
| | β -VAE [26] | \checkmark | 0.794 ± 0.02 | – | 0.783 ± 0.02 | – | 0.136 ± 0.07 | – |
| | ST-MEM [15] | \checkmark | <u>0.809 ± 0.02</u> | <u>0.791 ± 0.01</u> | <u>0.824 ± 0.03</u> | <u>0.793 ± 0.01</u> | <u>0.402 ± 0.10</u> | <u>0.253 ± 0.03</u> |
| Multimodal | Multimodal-CNN | \times | 0.753 ± 0.02 | 0.732 ± 0.01 | 0.681 ± 0.04 | 0.656 ± 0.04 | 0.173 ± 0.08 | 0.119 ± 0.04 |
| | MVAE [28] | \checkmark | 0.784 ± 0.02 | 0.790 ± 0.02 | 0.813 ± 0.03 | 0.805 ± 0.02 | 0.260 ± 0.13 | 0.274 ± 0.12 |
| | MoPoE-VAE [21] | \checkmark | 0.809 ± 0.03 | 0.771 ± 0.01 | 0.834 ± 0.03 | 0.787 ± 0.03 | 0.405 ± 0.08 | 0.258 ± 0.10 |
| | LS-EMVAE (ours) | \checkmark | 0.822 ± 0.01 | 0.815 ± 0.01 | 0.852 ± 0.02 | 0.814 ± 0.02 | 0.461 ± 0.03 | 0.412 ± 0.05 |
| Task-2: Phenotyping pre-/post-capillary PH | | | | | | | | |
| Unimodal | Resnet1d [9] | \times | 0.652 ± 0.03 | 0.593 ± 0.13 | 0.805 ± 0.04 | 0.761 ± 0.05 | 0.266 ± 0.08 | 0.243 ± 0.06 |
| | xResnet1d [19] | \times | 0.829 ± 0.02 | 0.813 ± 0.01 | 0.864 ± 0.05 | 0.798 ± 0.06 | 0.309 ± 0.12 | 0.276 ± 0.16 |
| | β -VAE [26] | \checkmark | 0.822 ± 0.03 | – | 0.846 ± 0.04 | – | 0.094 ± 0.05 | – |
| | ST-MEM [15] | \checkmark | <u>0.852 ± 0.02</u> | <u>0.844 ± 0.02</u> | <u>0.874 ± 0.03</u> | <u>0.816 ± 0.01</u> | <u>0.437 ± 0.11</u> | <u>0.346 ± 0.04</u> |
| Multimodal | Multimodal-CNN | \times | 0.753 ± 0.02 | 0.751 ± 0.01 | 0.545 ± 0.03 | 0.554 ± 0.02 | 0.049 ± 0.06 | 0.032 ± 0.02 |
| | MVAE [28] | \checkmark | 0.845 ± 0.02 | 0.855 ± 0.01 | 0.841 ± 0.01 | 0.836 ± 0.02 | 0.477 ± 0.04 | 0.469 ± 0.03 |
| | MoPoE-VAE [21] | \checkmark | 0.848 ± 0.01 | 0.836 ± 0.01 | 0.820 ± 0.03 | 0.792 ± 0.05 | 0.441 ± 0.08 | 0.373 ± 0.03 |
| | LS-EMVAE (ours) | \checkmark | 0.855 ± 0.01 | 0.869 ± 0.01 | 0.890 ± 0.03 | 0.863 ± 0.03 | 0.606 ± 0.04 | 0.544 ± 0.07 |

in the 6L-ECG setting, where LS-EMVAE outperforms all unimodal method baselines on both downstream tasks, achieving AUROC improvements ranging from $\Delta 0.078$ to $\Delta 0.013$ in PH detection and from $\Delta 0.309$ to $\Delta 0.027$ in PH phenotyping. These results confirm that the multimodal approach and latent distribution parameter fusion strategy in our model improve performance by effectively incorporating lead-specific features alongside shared features across both downstream tasks in 12L-ECG and 6L-ECG settings.

Multimodal Method Study: We compared LS-EMVAE with three multimodal methods. The Multimodal-CNN model is included to demonstrate the effectiveness of pre-training in LS-EMVAE, as it uses the same backbone and classification layers as LS-EMVAE but without pre-training. The other two methods are MVAE and MoPoE. Among them only MoPoE captures both lead-specific and shared features. Our LS-EMVAE outperforms MVAE and MoPoE in both downstream tasks across 12L-ECG and 6L-ECG settings. By outperforming MoPoE, it shows that our latent distribution parameter fusion aligns lead-specific and shared features seamlessly due to the effectiveness of our cross-modality alignment regularization loss.

Comparison of 6L-ECG and 12L-ECG: We further analyze the performance of 6L-ECG relative to 12L-ECG. The results show that 6L-ECG performs on par with 12L-ECG, with only a small performance gap. For instance, with the best-performing model, LS-EMVAE, the AUROC difference between 6L-ECG and 12L-ECG is only $\Delta 0.038$ and $\Delta 0.027$ for the two downstream tasks, respectively. The cost of implementing 12L-ECG in areas without diagnostic tools is significantly higher than that of 6L-ECG. Thus, 6L-ECG integrated with our

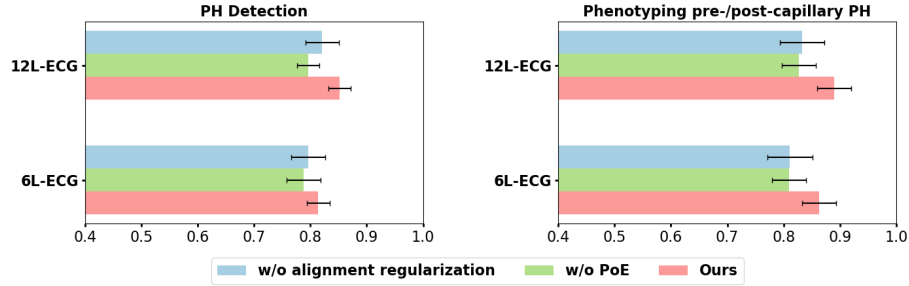


Fig. 2: Effectiveness of cross-modality alignment regularization loss and PoE in latent distribution parameter fusion. Each score indicates AUROC metric.

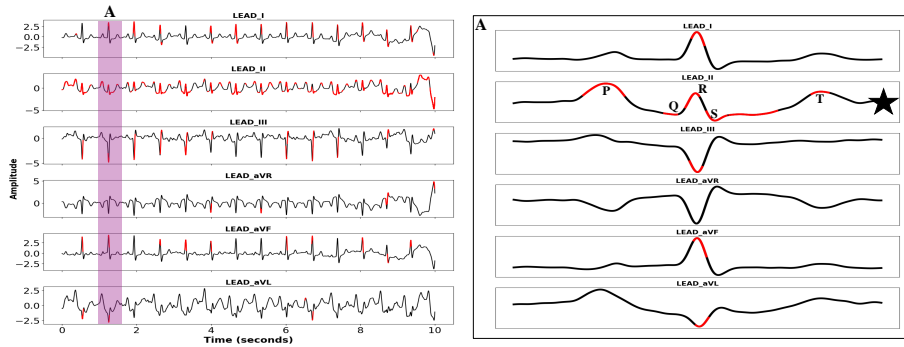


Fig. 3: Interpretability of LS-EMVAE for a PH patient identified by our model, with Lead-II (★) being the most important for PH detection.

LS-EMVAE model can be introduced in these areas as a cost-effective solution for faster and easier screening of PH patients.

Ablation Study: Fig. 2 shows the impact of the cross-modality alignment regularization loss and PoE in LS-EMVAE. We perform an ablation study on both downstream tasks in 12L-ECG and 6L-ECG settings and evaluate the AUROC. The results show that removing the cross-modality alignment regularization loss significantly reduces performance, as the model loses proper alignment between lead-specific and shared ECG features. Similarly, without PoE, the model fails to effectively inject shared features into the latent space. This demonstrates the importance of these two key components in our model.

Model Interpretation: In Fig. 3, we use integrated gradients [20] to illustrate the interpretability of LS-EMVAE in the 6L-ECG setting. The figure highlights important regions in red for a PH patient, identified by our model. The visualization shows that Lead-II is most important for PH detection, focusing on the P-wave and T-wave peaks, reflecting atrial depolarization and ventricular repolarization, which are commonly affected in PH due to right atrial enlargement

and right ventricular strain. The model also highlights the QRS complex in Lead-II, indicating right ventricular hypertrophy and right-axis deviation, along with the R-peak in other leads, signaling right ventricular overload and hypertrophy.

4 Conclusion

This paper presented a multimodal lead-specific ECG modeling approach for PH detection and phenotyping. We demonstrated that 1) our multimodal approach outperforms existing baselines in detecting and phenotyping PH across both 12L-ECG and 6L-ECG settings, providing a cost-effective solution for faster and more accessible PH screening in areas with both limited and no diagnostic tools, 2) incorporating lead-specific features alongside shared features with better alignment between them is important for improved PH prediction performance, and 3) the interpretations generated by our model are clinically relevant and can aid in decision-making, as validated by a clinician.

References

1. Alemi, A., Poole, B., Fischer, I., Dillon, J., Sauros, R.A., Murphy, K.: Fixing a broken elbow. In: International Conference on Machine Learning. pp. 159–168. PMLR (2018)
2. AliveCor Inc.: Kardiamobile 6l (2023), <https://www.kardia.com/kardiamobile-6l>, accessed April 24, 2023
3. Bu, Y., Zou, S., Liang, Y., Veeravalli, V.V.: Estimation of kl divergence: Optimal minimax rate. *IEEE Transactions on Information Theory* **64**(4), 2648–2674 (2018)
4. Godfrey, L.B.: An evaluation of parametric activation functions for deep learning. In: 2019 IEEE International Conference on Systems, Man and Cybernetics (SMC). pp. 3006–3011. IEEE (2019)
5. Gow, B., Pollard, T., Nathanson, L.A., Johnson, A., Moody, B., Fernandes, C., Greenbaum, N., Berkowitz, S., Moukheiber, D., Eslami, P., et al.: MIMIC-IV-ECG-Diagnostic Electrocardiogram Matched Subset. Type: dataset (2023)
6. Henkens, I.R., Scherp tong, R.W., van Kralingen, K.W., Said, S.A., Vliegen, H.W.: Pulmonary hypertension: the role of the electrocardiogram. *Netherlands Heart Journal* **16**(7), 250–254 (2008)
7. Higgins, I., Matthey, L., Pal, A., Burgess, C., Glorot, X., Botvinick, M., Mohamed, S., Lerchner, A.: beta-vae: Learning basic visual concepts with a constrained variational framework. In: International Conference on Learning Representations (2016)
8. Hinton, G.E.: Training products of experts by minimizing contrastive divergence. *Neural Computation* **14**(8), 1771–1800 (2002)
9. Hong, S., Xu, Y., Khare, A., Priambada, S., Maher, K., Aljiffry, A., Sun, J., Tumanov, A.: Holmes: Health online model ensemble serving for deep learning models in intensive care units. In: Proceedings of the 26th ACM SIGKDD International Conference on Knowledge Discovery & Data Mining. pp. 1614–1624 (2020)
10. Kusunose, K., Hirata, Y., Tsuji, T., Kotoku, J., Sata, M.: Deep learning to predict elevated pulmonary artery pressure in patients with suspected pulmonary hypertension using standard chest X ray. *Scientific Reports* **10**(1), 19311 (2020)

11. Lawry Aguila, A., Chapman, J., Altmann, A.: Multi-modal variational autoencoders for normative modelling across multiple imaging modalities. In: International Conference on Medical Image Computing and Computer-Assisted Intervention. pp. 425–434. Springer (2023)
12. Lin, T.Y., Goyal, P., Girshick, R., He, K., Dollár, P.: Focal loss for dense object detection. In: Proceedings of the IEEE International Conference on Computer Vision. pp. 2980–2988 (2017)
13. Loshchilov, I., Hutter, F.: Decoupled weight decay regularization. In: International Conference on Learning Representations (2017)
14. Maarman, G.J., Shaw, J., Allwood, B.: Pulmonary hypertension in majority countries: opportunities amidst challenges. *Current Opinion in Pulmonary Medicine* **26**(5), 373–383 (2020)
15. Na, Y., Park, M., Tae, Y., Joo, S.: Guiding masked representation learning to capture spatio-temporal relationship of electrocardiogram. In: The Twelfth International Conference on Learning Representations (2024)
16. Paszke, A., Gross, S., Massa, F., Lerer, A., Bradbury, J., Chanan, G., Killeen, T., Lin, Z., Gimelshein, N., Antiga, L., et al.: Pytorch: An imperative style, high-performance deep learning library. *Advances in Neural Information Processing Systems* **32** (2019)
17. Schlesinger, D.E., Diamant, N., Raghu, A., Reinertsen, E., Young, K., Batra, P., Pomerantsev, E., Stultz, C.M.: A deep learning model for inferring elevated pulmonary capillary wedge pressures from the 12-lead electrocardiogram. *JACC: Advances* **1**(1), 100003 (2022)
18. Shazeer, N., Mirhoseini, A., Maziarz, K., Davis, A., Le, Q., Hinton, G., Dean, J.: Outrageously large neural networks: The sparsely-gated mixture-of-experts layer. In: International Conference on Learning Representations (2017)
19. Strodthoff, N., Wagner, P., Schaeffter, T., Samek, W.: Deep learning for ecg analysis: Benchmarks and insights from ptb-xl. *IEEE Journal of Biomedical and Health Informatics* **25**(5), 1519–1528 (2020)
20. Sundararajan, M., Taly, A., Yan, Q.: Axiomatic attribution for deep networks. In: International Conference on Machine Learning. pp. 3319–3328. PMLR (2017)
21. Sutter, T.M., Daunhawer, I., Vogt, J.E.: Generalized multimodal ELBO. In: International Conference on Learning Representations (2021)
22. Suvon, M.N., Tripathi, P.C., Fan, W., Zhou, S., Liu, X., Alabed, S., Osmani, V., Swift, A.J., Chen, C., Lu, H.: Multimodal variational autoencoder for low-cost cardiac hemodynamics instability detection. In: International Conference on Medical Image Computing and Computer-Assisted Intervention. pp. 296–306. Springer (2024)
23. Traversi, E., Cobelli, F., Pozzoli, M.: Doppler echocardiography reliably predicts pulmonary artery wedge pressure in patients with chronic heart failure even when atrial fibrillation is present. *European Journal of Heart Failure* **3**(2), 173–181 (2001)
24. Tripathi, P.C., Suvon, M.N., Schobs, L., Zhou, S., Alabed, S., Swift, A.J., Lu, H.: Tensor-based multimodal learning for prediction of pulmonary arterial wedge pressure from cardiac mri. In: International Conference on Medical Image Computing and Computer-Assisted Intervention. pp. 206–215. Springer (2023)
25. Tripathi, P.C., Tabakhi, S., Suvon, M.N., Schöb, L., Alabed, S., Swift, A.J., Zhou, S., Lu, H.: Interpretable multimodal learning for cardiovascular hemodynamics assessment. *arXiv preprint arXiv:2404.04718* (2024)
26. van der Valk, V., Atsma, D., Scherptong, R., Staring, M.: Joint optimization of a β -vae for ecg task-specific feature extraction. In: International Conference on Med-

- ical Image Computing and Computer-Assisted Intervention. pp. 554–563. Springer (2023)
27. Welch, B.L.: The generalization of ‘student’s’ problem when several different population variances are involved. *Biometrika* **34**(1-2), 28–35 (1947)
 28. Wu, M., Goodman, N.: Multimodal generative models for scalable weakly-supervised learning. *Advances in Neural Information Processing Systems* **31** (2018)
 29. Zhang, H., Liu, W., Shi, J., Chang, S., Wang, H., He, J., Huang, Q.: Maefe: Masked autoencoders family of electrocardiogram for self-supervised pretraining and transfer learning. *IEEE Transactions on Instrumentation and Measurement* **72**, 1–15 (2022)